

Article

Simulating the Hysteretic Characteristics of Hard Magnetic Materials Based on $\text{Nd}_2\text{Fe}_{14}\text{B}$ and $\text{Ce}_2\text{Fe}_{14}\text{B}$ Intermetallics

Natalia B. Kolchugina ^{1,*}, Mark V. Zheleznyi ^{1,2}, Aleksandr G. Savchenko ², Vladimir P. Menushenkov ², Gennadii S. Burkhanov ¹, Yurii S. Koshkid'ko ^{1,3} , Jacek Ćwik ³ , Nikolai A. Dormidontov ¹, Katerina Skotnicova ⁴ , Miroslav Kursa ⁴ and Pavel A. Prokofev ^{1,5}

¹ Baikov Institute of Metallurgy and Materials Science, Russian Academy of Sciences, Leninskii pr. 49, 119334 Moscow, Russia; markiron@mail.ru (M.V.Z.); gburkhanov@imet.ac.ru (G.S.B.); y.koshkidko@intibs.pl (Y.S.K.); ontip@mail.ru (N.A.D.); pav3387@yandex.ru (P.A.P.)

² National University of Science and Technology MISiS, Leninskii pr. 4, 119991 Moscow, Russia; algsav@gmail.com (A.G.S.); menushenkov@gmail.com (V.P.M.)

³ Institute of Low Temperature and Structure Research, Polish Academy of Sciences, ul. Okólna 2, 50-422 Wrocław, Poland; j.cwik@intibs.pl

⁴ VSB—Technical University of Ostrava, Faculty of Materials Science and Technology, 17. listopadu 2172/15, 70800 Ostrava, Czech Republic; Katerina.Skotnicova@vsb.cz (K.S.); Miroslav.Kursa@vsb.cz (M.K.)

⁵ JSC Spetsmagnit, Dmitrovskoe sh. 58, 127238 Moscow, Russia

* Correspondence: nkolchugina@imet.ac; Tel.: +7-(499)135-96-15

Received: 12 May 2020; Accepted: 14 June 2020; Published: 17 June 2020



Abstract: The $\text{Ce}_2\text{Fe}_{14}\text{B}$ intermetallic, like $\text{Nd}_2\text{Fe}_{14}\text{B}$, has the tetragonal $\text{Nd}_2\text{Fe}_{14}\text{B}$ -type structure (space group $P4_2/mnm$), in which Ce ions have a mixed-valence state characterized by the coexistence of trivalent $4f^1$ and tetravalent $4f^0$ electron states. Despite the fact that the saturation magnetization, magnetic anisotropy field, and Curie temperature of the $\text{Ce}_2\text{Fe}_{14}\text{B}$ intermetallic are substantially lower than those of $\text{Nd}_2\text{Fe}_{14}\text{B}$ and $\text{Pr}_2\text{Fe}_{14}\text{B}$, $\text{Ce}_2\text{Fe}_{14}\text{B}$ retains the capacity of being able to be used in the manufacturing of rare-earth permanent magnets. Moreover, at low temperatures, the anisotropy field of $\text{Ce}_2\text{Fe}_{14}\text{B}$ is higher than that of $\text{Nd}_2\text{Fe}_{14}\text{B}$, and $\text{Ce}_2\text{Fe}_{14}\text{B}$ does not undergo the spin-reorientation transition. In this respect, studies of (Nd, Ce)-Fe-B alloys, which are intended for the improvement of the service characteristics-to-cost ratio, are very relevant. A model and algorithm for calculating the hysteresis loops of uniaxial hard magnetic materials with allowance for the K_1 and K_2 ($K_2 > 0$ and $K_1 > 0$ and $K_1 < 0$) magnetic anisotropy constants were developed and allowed us to obtain data on their effect on the parameters of hysteresis loops for a wide temperature range (0–300 K). The simulation and analysis of hysteresis loops of the quasi-ternary intermetallics $(\text{Nd}_{1-x}\text{Ce}_x)_2\text{Fe}_{14}\text{B}$ ($x = 0-1$) was performed. Results of the simulation indicate that the alloying of the $\text{Nd}_2\text{Fe}_{14}\text{B}$ intermetallic with Ce to $x = 0.94$ (1) does not completely eliminate the negative effect of spin-reorientation phase transition on the residual magnetization of the $(\text{Nd}_{1-x}\text{Ce}_x)_2\text{Fe}_{14}\text{B}$ intermetallic and (2) slightly decreases the slope of magnetization reversal curve.

Keywords: R-Fe-B intermetallics; cerium; permanent magnets; simulation; magnetic anisotropy constant; hysteresis loop; coercive force; residual magnetization

1. Introduction

In recent years, the low cost of Ce-containing Nd-Fe-B permanent magnets, in some areas being a potential alternative to those based on expensive rare-earth elements (Nd, Pr, Dy, Tb), has stimulated considerable research efforts [1,2].

Similar to the other R-Fe-B systems, the Ce-Fe-B system is characterized by the formation of the ternary intermetallic compound having a 2:14:1 stoichiometry and tetragonal $\text{Nd}_2\text{Fe}_{14}\text{B}$ -type structure (space group $P4_2/mnm$) [3]. The unit cell contains four formula units comprising 68 atoms: there are six crystallographic iron sites ($16k_1$, $16k_2$, $8j_1$, $8j_2$, $4c$, $4e$), two rare-earth metal sites ($4f$, $4g$), and one boron site ($4g$). Table 1 shows the lattice parameters of the $\text{R}_2\text{Fe}_{14}\text{B}$ compounds with $\text{R} = \text{Nd}$, Pr , and Ce and their principal magnetic characteristics. This shows that both the a and c lattice parameters of the $\text{Ce}_2\text{Fe}_{14}\text{B}$ compound are slightly lower than those of the $\text{Nd}_2\text{Fe}_{14}\text{B}$ and $\text{Pr}_2\text{Fe}_{14}\text{B}$ compounds [4].

Table 1. Saturation magnetization I_s , magnetic anisotropy field H_A , lattice parameters a and c , and Curie temperature T_C of the $\text{R}_2\text{Fe}_{14}\text{B}$ compounds with $\text{R} = \text{Ce}$, Pr , Nd at room temperature.

Compound	I_s , T	H_A , kOe	T_C , K	a , nm	c , nm	Reference
$\text{Nd}_2\text{Fe}_{14}\text{B}$	1.61	73	585	0.880	1.220	[4,5]
$\text{Pr}_2\text{Fe}_{14}\text{B}$	1.56	87	565	0.880	1.223	[4,6]
$\text{Ce}_2\text{Fe}_{14}\text{B}$	1.17	26	424	0.876	1.211	[4,7]

The anisotropy of the $\text{Nd}_2\text{Fe}_{14}\text{B}$ compound is dominated by the rare-earth atoms that occupy two inequivalent sites, $4f$ and $4g$, of the tetragonal structure [8,9]. One Nd site (g) strongly prefers the $[001]$ direction at ambient temperature and dictates the macroscopic easy-axis direction. The other Nd site (f) (containing half of all the Nd atoms) reduces the intrinsic stability by favoring alignment along $[110]$ -type directions (basal plane). The results indicate that coercivity may be enhanced by preferential chemical doping of Nd f sites. $\text{Nd}_2\text{Fe}_{14}\text{B}$ is characterized by the uniaxial state at temperatures above the spin-reorientation temperature T_{sr} . $\text{Ce}_2\text{Fe}_{14}\text{B}$ exhibits the uniaxial magnetic anisotropy over the whole temperature range of ferromagnetic ordering [10]. Its uniaxial anisotropy is higher than that of $\text{R}_2\text{Fe}_{14}\text{B}$ with $\text{R} = \text{La}$, Lu , Y [10], but lower than that of $\text{Nd}_2\text{Fe}_{14}\text{B}$ at temperatures substantially higher than the spin-reorientation temperature. It was predicted [11] that, theoretically, Ce atoms in the $(\text{Nd}_{1-x}\text{Ce}_x)_2\text{Fe}_{14}\text{B}$ compounds occupy the $4g$ positions (large in volume); this is explained by atomic size effects. However according to [8], $4f$ position (smaller in volume) is preferred for the Ce atoms.

Taking into account the fact that Ce prefers $4f$ positions, the progressive substitution of Ce for Nd should decrease the easy magnetization axis (EMA) cone opening. Thus, the formation of a uniaxial state can occur even in the presence of a small amount of Nd in $(\text{Nd}_{1-x}\text{Ce}_x)_2\text{Fe}_{14}\text{B}$. At present, no experimental data confirming the assumption are available. In turn, when assuming that Ce atoms prefer $4g$ positions, it is possible to conclude that the cone opening will be smaller for low substitutions of Ce for Nd. Because of this, T_{sr} varies slightly for low Ce contents. A small change in T_{sr} for the Ce substitution to $x = 0.3$ was observed in [12]. According to the data from [8], the magnetocrystalline anisotropy of $\text{Nd}_2\text{Fe}_{14}\text{B}$ remains when Ce substitutes for Nd up to 20%. The further increase in the Ce content decreases the uniaxial magnetic anisotropy energy.

The uniaxial anisotropy found in $\text{Ce}_2\text{Fe}_{14}\text{B}$ is attributed mainly to the magnetism of Fe [8]. Alloying Ce on R-sites in $(\text{Nd}_{1-x}\text{Ce}_x)_2\text{Fe}_{14}\text{B}$ barely affects the Fe moments. Nd magnetization changes orientation at $x > 0.5$, with a larger antiferromagnetic moment on $4f$ sites compared to $4g$ sites. Such a transition of the Nd magnetic state causes an overall reduction of the net magnetization of the cell, and is the reason for instability at higher percentage Ce [11]. The magnetic moment of rare-earth sublattice is mainly determined by Nd atoms. The temperature behavior of magnetization of $\text{R}_2\text{Fe}_{14}\text{B}$ with $\text{R} = \text{Nd}$, Ce was studied in [12].

The metallurgical behavior, heat treatment conditions, fundamental characteristics, and magnetic properties of the $\text{Nd}_2\text{Fe}_{14}\text{B}$ and $\text{Ce}_2\text{Fe}_{14}\text{B}$ intermetallics differ substantially although the compounds have the same crystal structure. The existence of the CeFe_2 phase determines the principal difference in the ternary Nd-Fe-B and Ce-Fe-B phase diagrams [3,13]. Cerium ions in the $\text{Ce}_2\text{Fe}_{14}\text{B}$ intermetallic have a mixed-valence state, namely, the trivalent $4f^1$ and tetravalent $4f^0$ electron states coexist [14].

According to data from [15], the hysteretic properties of Nd-Ce-Fe-B magnets decrease as the Ce content increases. However, the squareness of the magnetization reversal curve remains high [16–18], and the magnetic characteristics remain adequate when the Ce content does not exceed 10%.

Usually, it is assumed that the decrease in the magnetic characteristics of Ce-containing Nd₂Fe₁₄B alloys is due to the lower magnetic properties of Ce₂Fe₁₄B as compared to those of Nd₂Fe₁₄B (see Table 1). However, according to data from [18,19], an anomalous increase in the coercive force was found by studying the effect of Ce substitution for Nd on the magnetic properties and microstructure of sintered magnets. Pathak et al. [20] reported that the substitution of 20% Ce for Nd in the ternary Nd₂Fe₁₄B alloy allowed the authors to reach a sufficiently high coercive force ($H_{ci} = 10$ kOe), which exceeds that of Nd₂Fe₁₄B ($H_{ci} = 8.3$ kOe).

Currently, the development of high-coercivity, high-performance permanent magnets operating in a wide temperature range, in particular at low and cryogenic temperatures, is of importance. Nd-Fe-B magnets are unsuitable for operation at such temperatures. The EMA of the Nd₂Fe₁₄B compound at 4.2 K is in the [110] plane and makes the angle $\theta \approx 30^\circ$ with the c axis. As the temperature increases, the transition to the collinear structure takes place at the spin-reorientation temperature $T_{sr} = 135\text{--}138$ K [21]. Below this temperature, the magnetic moment deviates from the c axis, the first magnetic anisotropy constant K_1 passes zero and changes the sign from positive to negative, whereas the second magnetic anisotropy constant remains positive ($K_2 > 0$). As a result, below T_{sr} , the experimental magnetization reversal curves in negative magnetic fields exhibit a bending, which increases with decreasing temperature. In this case, the residual magnetization and maximum energy product decrease abruptly.

At room temperature, the magnetic properties of Ce₂Fe₁₄B are substantially lower than those of Nd₂Fe₁₄B, whereas, at cryogenic temperatures, the magnetic anisotropy field of Ce₂Fe₁₄B is markedly higher than that of Nd₂Fe₁₄B. Moreover, it is of importance that Ce₂Fe₁₄B does not have a spin-reorientation transition. Thus, it is reasonable to expect that the partial substitution of Ce for Nd in the Nd₂Fe₁₄B compound can lead to the improvement of the hysteretic characteristics of permanent magnets based on the quasi-ternary (Nd, Ce)₂Fe₁₄B intermetallics.

Data on the effect of Ce substitution for Nd on the spin-reorientation transition temperature of the Nd_{2-x}Ce_xFe₁₄B single crystals are available in [22], where the evolution of the spin-reorientation temperature as a function of the Ce concentration up to $x = 0.4$ is considered. The spin-reorientation temperature decreases by only about 6% when Ce substitutes for 38% of Nd. It is shown that T_{sr} is suppressed much more rapidly for higher x . It is likely that the population of REM sites (4g or 4f) is responsible for the spin-reorientation [22].

Taking into account the absence of systematic data on this problem in the literature, the present study is aimed at the simulation of hysteretic properties of the (Nd_{1-x}Ce_x)₂Fe₁₄B intermetallics in order to determine the optimum alloyed compositions. The simulation and analysis of hysteresis loops of the (Nd_{1-x}Ce_x)₂Fe₁₄B ($x = 0\text{--}1$) compounds are performed for a temperature range of 0 to 300 K.

2. Algorithm and Model for Calculating the Hysteresis Loops of Hard Magnetic Materials with the Uniaxial Tetragonal Lattice

The resulting magnetization vector I_s at each point of a crystalline ferromagnet is simultaneously oriented along certain crystallographic directions (EMAs). In order to rotate I_s to another direction, magnetic field H should be applied along this direction, and work should be done. This work makes sense of the anisotropy energy E_a , which, for magnets with the uniaxial tetragonal lattice, is given by the expression:

$$E_a = -K_1 \cos^2(\varphi) - K_2 \cos^4(\varphi), \quad (1)$$

where K_1 and K_2 are the first and second magnetic anisotropy constants, respectively, and φ_a is the angle made by the EMA and I_s . The anisotropy constants are proportional to the work, which should be done to rotate the magnetization from the EMA direction to the hard magnetization axis direction.

To take into account the cooperative effect of magnetic anisotropy and magnetic field, we considered a single crystal in the form of a plain disk oriented along a certain crystallographic plane. When the magnetic field is applied along the plane, the magnetization is also within the plane. It is assumed that the magnetization of the body is uniform and domains are absent.

When applying magnetic field H , the position of I_s also determined by the magnetic field energy:

$$E_H = -H I_s \cos(\varphi), \quad (2)$$

where φ_H is the angle made by the vectors. In the end, I_s takes a position corresponding to the minimum summary energy:

$$E = E_a + E_H \quad (3)$$

In terms of the model and algorithm [23] (program Hysteresis developed by Associate Prof. V.L. Stolyarov) used for the simulation of magnetic hysteresis loops of $(Nd_{1-x}Ce_x)_2Fe_{14}B$ intermetallics with the uniaxial tetragonal lattice, the following initial parameters are inputted: α is the angle made by an arbitrary plane and the X-axis [100] and the external magnetic field H is applied in this plane, θ_H is the angle made by the H field direction and Z-axis [001]. The following parameters are counted and outputted: θ is the angle made by the Z-axis [0001] and EMA, φ_a is the angle made by the EMA and I_s ; and angle φ_H .

Calculation of the position of the magnetization vector I_s for an arbitrary vector H , at which the total energy is minimal (Equation (3)), allows us to calculate the projection of the magnetization on the field direction $I = I_s \cos(\varphi_H)$ and to construct the magnetization curve $I = I(H)$.

3. Results and Discussion

3.1. Determination of Magnetic Anisotropy Constants, Normalized Ratio of Anisotropy Constants (K_2/K_1), and Angle of the EMA cone in Calculating Hysteresis Loops of the $(Nd_{1-x}Ce_x)_2Fe_{14}B$ Intermetallics with $0 \leq x \leq 1$

Temperature dependences of the magnetic anisotropy constants K_1 and K_2 of $Nd_2Fe_{14}B$ in a temperature range of 0–500 K are available in [24]. The sign of K_1 alternates at the spin-reorientation transition temperature $T_{sr} = 135$ K. Below this temperature, the preferred direction of EMA begins to deviate from the c axis direction (Z-axis [001]) of the tetragonal crystal lattice, and the angle (θ) of the EMA cone for each temperature is given by the expression:

$$\sin^2(\theta(T)) = -\frac{K_1(T)}{2 K_2(T)} \quad (4)$$

At 4.2 K, this angle reaches $\sim 30^\circ$ [24].

The temperature dependences of the magnetic anisotropy constant K_1 and K_2 of $Ce_2Fe_{14}B$ in a temperature range of 0–300 K are available in [25]. Unlike the magnetic anisotropy constants of $Nd_2Fe_{14}B$, K_1 and K_2 of $Ce_2Fe_{14}B$ remain positive within the 0–300 K temperature range. The absolute values of K_1 and K_2 of $Ce_2Fe_{14}B$ are substantially lower than those of $Nd_2Fe_{14}B$.

To calculate the anisotropy constants of the quasi-ternary intermetallics $(Nd_{1-x}Ce_x)_2Fe_{14}B$ with $0 \leq x \leq 1$ at different temperatures, the literature data on the anisotropy constants of $Nd_2Fe_{14}B$ and $Ce_2Fe_{14}B$ and the following linear expressions were used:

$$K_1(T, x) = (1-x) K_1(T)_{Nd_2Fe_{14}B} + x K_1(T)_{Ce_2Fe_{14}B} \quad (5)$$

$$K_2(T, x) = (1-x) K_2(T)_{Nd_2Fe_{14}B} + x K_2(T)_{Ce_2Fe_{14}B} \quad (6)$$

The ratio of anisotropy constants K_2 to K_1 and the θ angle (made by the EMA and c axis) were calculated by the expressions:

$$\frac{K_2(T, x)}{|K_1(T, x)|} \quad (7)$$

at $K_1(T, x) < 0$

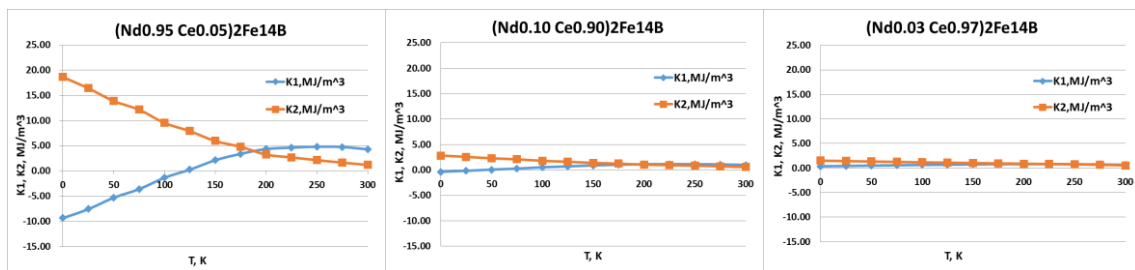
$$\theta(T) = \arcsin\left(\sqrt{-\frac{K_1(T)}{2K_2(T)}}\right) \quad (8)$$

at $K_1(T, x) \geq 0$

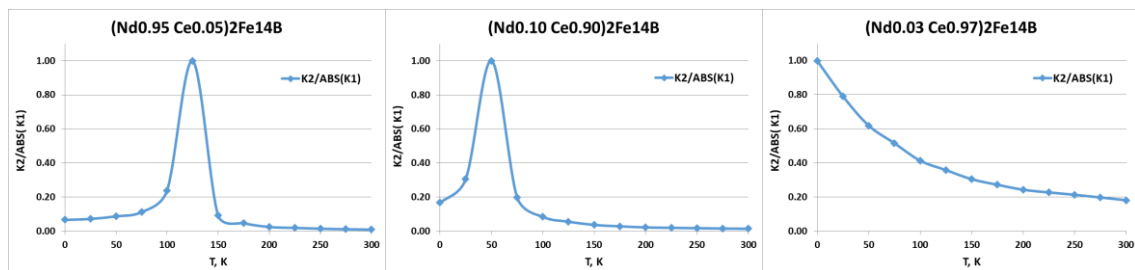
$$\theta(T, x) = 0 \quad (9)$$

The following composition ranges of $(\text{Nd}_{1-x}\text{Ce}_x)_2\text{Fe}_{14}\text{B}$ were considered: (1) $x = 0, 0.05, 0.10, 0.15, 0.20, 0.25, 0.30, 0.35, 0.40, 0.45, 0.50, 0.55, 0.60, 0.65, 0.70, 0.75$; (2) $x = 0.80, 0.85; 0.90, 0.91, 0.92$ and (3) $x = 0.93, 0.94, 0.95, 0.96, 0.97, 0.98, 0.99, 1.00$.

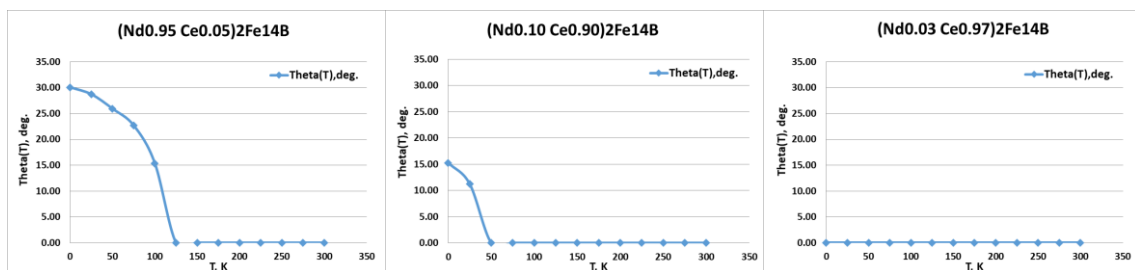
The calculated temperature dependences of the magnetic anisotropy constants, their ratio, and temperature dependences of the θ angle for $(\text{Nd}_{1-x}\text{Ce}_x)_2\text{Fe}_{14}\text{B}$ with $x = 0.05, 0.90$, and 0.97 are given in Figure 1, as an example. The compositional dependences of the spin-reorientation temperature (T_{SR}) of $(\text{Nd}_{1-x}\text{Ce}_x)_2\text{Fe}_{14}\text{B}$ are given in Figure 2.



(a)



(b)



(c)

Figure 1. Temperature dependences of the (a) K_1 and K_2 magnetic anisotropy constants, (b) normalized $K_2/|K_1|$ ratio, and (c) θ angle for $(\text{Nd}_{1-x}\text{Ce}_x)_2\text{Fe}_{14}\text{B}$ with $x = 0.05$ (first composition range), 0.90 (second composition range), and 0.97 (third composition range).

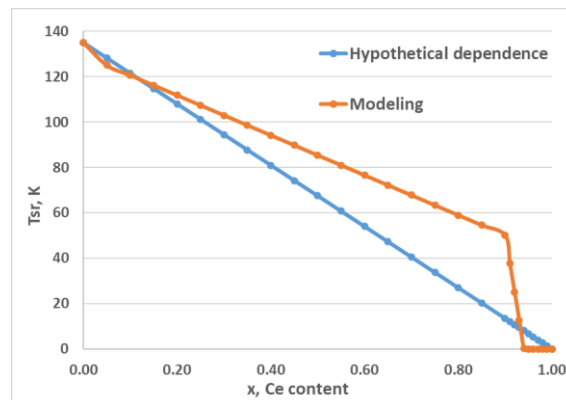


Figure 2. Compositional dependences of spin-reorientation temperature (T_{sr}) of $(Nd_{1-x}Ce_x)_2Fe_{14}B$: (blue) hypothetical (linear) trend and (red) results of simulation (this work).

It is seen from Figures 1 and 2 that, as Ce substitutes for Nd in the range $x = 0$ – 0.75 (first composition range), the values of K_1 and K_2 constants decrease on average by $\sim 75\%$ and $\sim 99\%$, respectively. The temperature corresponding to the maximum of the normalized $K_2/|K_1|$ ratio decreases from 135 to 63 K. The temperature T_{sr} also decreases from 135 to 63 K. The highest value of the θ angle at 0 K decreases from 30.15° ($x = 0$) to 24.77° ($x = 0.75$).

As the Ce content in $(Nd_{1-x}Ce_x)_2Fe_{14}B$ increases in the range $x = 0.80$ – 0.92 (second composition range), the K_1 and K_2 values additionally decrease on average by $\sim 61\%$ and $\sim 63\%$, respectively. In turn, the temperature corresponding to the maximum of normalized $K_2/|K_1|$ ratio shifts from 59 to 25 K. The temperature T_{sr} also decreases from 59 to 25 K. The largest value of the θ angle at 0 K monotonically decreases from 23.12° ($x = 0.80$) to 11.03° ($x = 0.92$).

It is seen from the dependences given in Figures 1 and 2 that, as the cerium content in the $(Nd_{1-x}Ce_x)_2Fe_{14}B$ intermetallic increases from $x = 0.93$ to $x = 1.00$, the anisotropy constant K_2 additionally decreases by an average $\sim 35\%$, whereas the K_1 constant changes the sign from negative to positive. The T_{sr} temperature decreases from 13 to 0 K as the cerium content increases to $x = 0.94$. The temperature corresponding to the maximum of normalized $K_2/|K_1|$ ratio also decreases from 13 to 0 K. The highest value of the θ angle at 0 K decreases from 7.34° to 0° (at $x \geq 0.94$).

3.2. Simulation of Magnetization Curves and Hysteresis Loops of $(Nd_{1-x}Ce_x)_2Fe_{14}B$ with $x = 0.00$ – 1.00

The simulated hysteresis loops for $(Nd_{1-x}Ce_x)_2Fe_{14}B$ with $x = 0$ – 1.00 show that, as the applied magnetization reversing field reaches the coercive force H_c (at which the abrupt overturn of I_s takes place), the decrease in the hysteresis loop squareness is observed; the “rounding” becomes more substantial as the temperature decreases. Below T_{sr} , the decrease starts in the positive fields. Figure 3 shows the temperature dependences of the normalized and unnormalized residual magnetization (I_r/I_s and I_r) for the three composition ranges of the $(Nd_{1-x}Ce_x)_2Fe_{14}B$ compounds.

For all quasi-ternary compositions, the I_r/I_s ratio monotonically decreases with decreasing temperature. This is caused by the deviation of I_s from the EMA in the applied magnetic field H and the transition to the EMA cone below T_{sr} . Only for the high-cerium contents ($x \geq 0.94$), the I_r/I_s ratio remains unchanged and equal to 0.9999 (< 1.0000) for a certain temperature range.

For the composition range $x = 0$ – 0.75 (Figure 3a), as the temperature decreases from 300 K to $T_{sr}(x)$, I_r/I_s remains unchanged and equal to 0.9999 for all these compositions. This means that, after saturation, the magnetization remains parallel to the EMA and Z-axis as the external field decreases to zero. The monotonic progressive decrease in I_r/I_s is observed simultaneously with decreasing temperature below $T_{sr}(x)$ and Ce content x . For each Ce content x , the temperature dependences $I_r(T, x)$ have the maximum value in the range of $T_{sr}(x)$ (Figure 3b). The monotonic shift of the I_r maximum to low temperatures from $I_r(T = 135 \text{ K}, x = 0) = 191.6 \text{ A m}^2/\text{kg}$ to $I_r(T = 102 \text{ K}, x = 0.75) = 161.5 \text{ A m}^2/\text{kg}$ correlates with a similar shift of the maximum of normalized $K_2/|K_1|$ ratio and a decrease in $T_{sr}(x)$ with

increasing cerium content x (Figures 1 and 2). The maximum in these dependences is related to the competition of two physical phenomena, such as the monotonic increase in the total magnetic moment of $R_2Fe_{14}B$ intermetallics (where $R = Nd$ or Ce) with decreasing temperature and the spin-reorientation below the T_{sr} temperature.

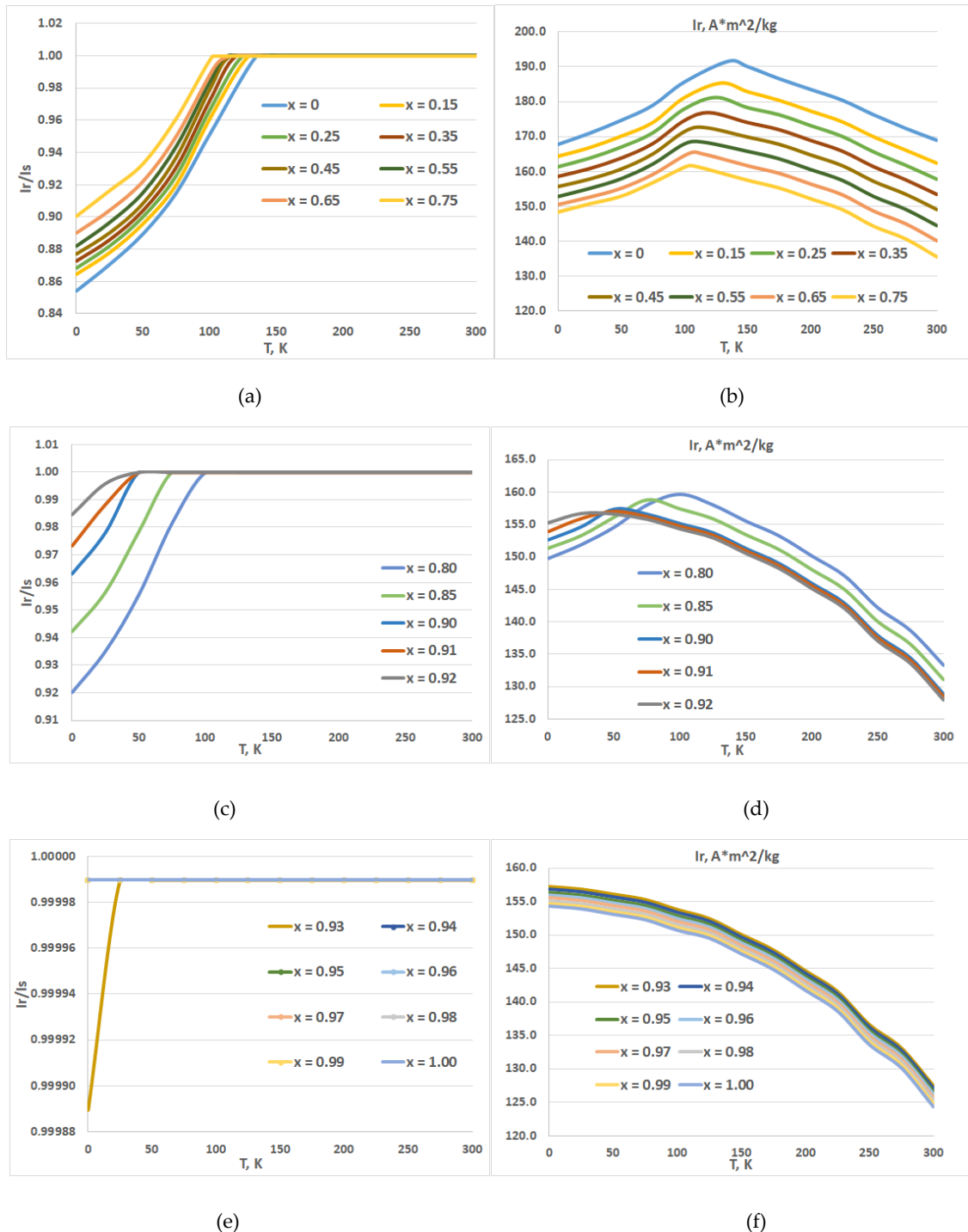


Figure 3. Temperature dependences of the normalized and unnormalized residual magnetization (I_r/I_s and I_r) of the $(Nd_{1-x}Ce_x)_2Fe_{14}B$ compounds with different x : (a) and (b) 0, 0.15, 0.25, 0.35, 0.45, 0.55, 0.65, 0.75; (c) and (d) 0.80, 0.85, 0.90, 0.91, 0.92; (e) and (f) 0.93, 0.94, 0.95, 0.96, 0.97, 0.98, 0.99, 1.00.

For the composition range $x = 0.80\text{--}0.92$ (Figure 3c), as the temperature decreases from 300 K to $T_{sr}(x)$, I_r/I_s remains equal to 0.9999 for all these compositions, i.e., the magnetization after saturation remains parallel to the EMA and Z-axis as the magnetizing field decreases to zero. The monotonic and progressive decrease in I_r/I_s is observed with simultaneously decreasing temperature below $T_{sr}(x)$ and Ce content x . For each Ce content x , the temperature dependences $I_r(T, x)$ also have the maximum in the range of $T_{sr}(x)$ (Figure 3d). The monotonic shift of the I_r maximum to the low temperature range from $I_r(T = 100\text{ K}, x = 0.80) = 159.6\text{ A m}^2/\text{kg}$ to $I_r(T = 25\text{ K}, x = 0.92) = 156.6\text{ A m}^2/\text{kg}$ correlates with the similar shift of the normalized K_2/K_1 ratio and a decrease in $T_{sr}(x)$ with increasing cerium content x (Figures 1 and 2). However, in this range of cerium concentrations, the temperature dependences of I_r overlap; the overlapping was not observed in the range $x = 0\text{--}0.75$ (Figure 3d). This interesting and anomalous change in I_r is also related to the “stronger” competition of a monotonic increase in the total magnetic moment of $R_2\text{Fe}_{14}\text{B}$ intermetallics (where $R = \text{Nd}$ or Ce) with decreasing temperature and the spin-reorientation below T_{sr} . Owing to the nature of the change in magnetic properties, the composition range $x = 0.80\text{--}0.92$ is intermediate between neodymium-based intermetallics and cerium-based intermetallics $R_2\text{Fe}_{14}\text{B}$.

Figure 3e shows the temperature dependences of the normalized residual magnetization for the third composition range of the $(\text{Nd}_{1-x}\text{Ce}_x)_2\text{Fe}_{14}\text{B}$ intermetallics with $x = 0.93\text{--}1.00$. As the temperature decreases from 300 K to 0 K, I_r/I_s remains equal to 0.9999 for all alloys with $x \geq 0.94$, i.e., after saturation, the magnetization remains parallel to the EMA and Z-axis as the magnetizing field decreases to zero. Only for the alloys with $0.93 \leq x < 0.94$, the monotonic and progressive decrease in I_r/I_s is observed as the simultaneous decrease in temperature below $T_{sr}(x)$ and decrease in the Ce concentration take place. As x increases from 0.94 to 1.00, the considered maximum of I_r shifts to zero and degenerates owing to the decreasing effect of the spin-reorientation. This effect also correlates with a similar shift of the normalized K_2/K_1 ratio and a decrease in $T_{sr}(x)$ with increasing cerium concentration x (Figures 1 and 2).

The considered features of the change of the residual magnetization clearly manifest themselves in the concentration dependence at $T = 0\text{ K}$. Figure 4 shows that the composition range $x = 0.80\text{--}0.92$ is intermediate between neodymium-based intermetallics and cerium-based intermetallic $R_2\text{Fe}_{14}\text{B}$ and is characterized by anomalous change in the residual magnetization.

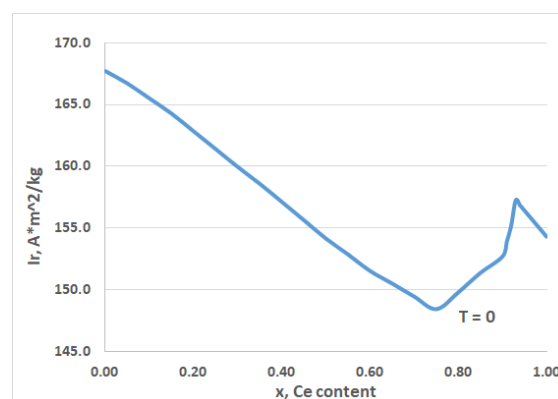


Figure 4. Compositional dependence of the residual magnetization I_r for the $(\text{Nd}_{1-x}\text{Ce}_x)_2\text{Fe}_{14}\text{B}$ compounds at $T = 0\text{ K}$.

Figure 5 shows temperature dependences of the coercive force H_c of the $(\text{Nd}_{1-x}\text{Ce}_x)_2\text{Fe}_{14}\text{B}$ compounds with $x = 0\text{--}1.00$.

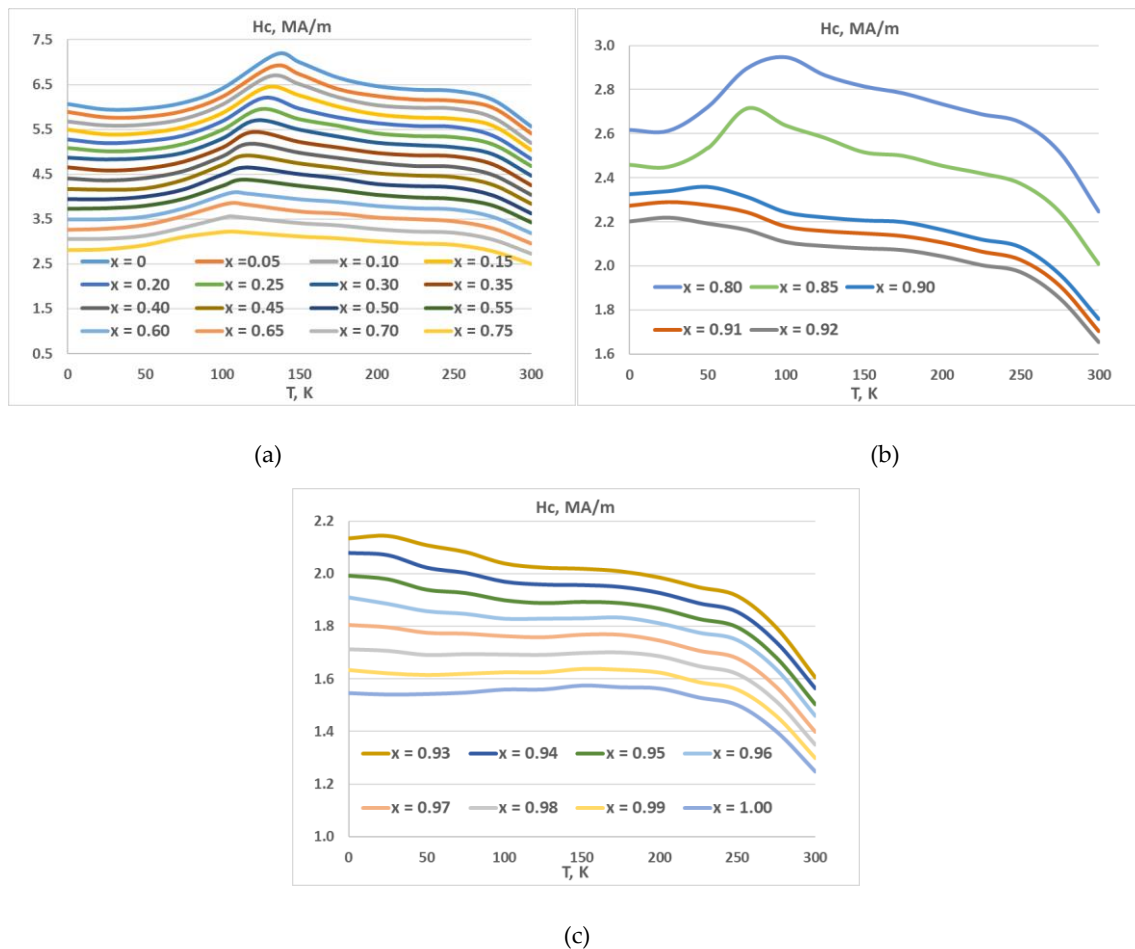


Figure 5. Temperature dependences of the coercive force H_c of the $(\text{Nd}_{1-x}\text{Ce}_x)_2\text{Fe}_{14}\text{B}$ compounds with different x : (a) 0, 0.05, 0.10, 0.15, 0.20, 0.25, 0.30, 0.35, 0.40, 0.45, 0.50, 0.55, 0.60, 0.65, 0.70, 0.75; (b) 0.80, 0.85, 0.90, 0.91, 0.92; and (c) 0.93, 0.94, 0.95, 0.96, 0.97, 0.98, 0.99, 1.00.

It is seen that, for each Ce content $x = 0$ –0.75, the coercive force H_c reaches the maximum value in the range of $T_{sr}(x)$ (Figure 5a). The monotonic shift of the H_c maximum to the low-temperature range from $H_c(T = 135 \text{ K}, x = 0) = 7.2 \text{ MA/m}$ to $H_c(T = 102 \text{ K}, x = 0.75) = 3.2 \text{ MA/m}$ correlates with a similar shift of the maximum of normalized K_2/K_1 ratio, shift of the maximum of I_r , and a decrease in $T_{sr}(x)$ with increasing cerium concentration x (Figures 1 and 3). The maximum in these dependences is related to the competition of two physical phenomena, such as the monotonic increase in the magnetic anisotropy field H_A of $\text{R}_2\text{Fe}_{14}\text{B}$ intermetallics (where $\text{R} = \text{Nd}$ or Ce) with decreasing temperature and the spin-reorientation below T_{sr} , that facilitates the magnetization reversal process in an external magnetic field.

As is seen, for each Ce content $x = 0.80$ –0.92 (Figure 5b), the coercive force H_c reaches the maximum value in a temperature range of $T_{sr}(x)$. The monotonic shift of the H_c maximum to the low-temperature range from $H_c(T = 100 \text{ K}, x = 0.80) = 2.9 \text{ MA/m}$ to $H_c(T = 25 \text{ K}, x = 0.92) = 2.2 \text{ MA/m}$ correlates with a similar shift of the maximum of the normalized K_2/K_1 ratio, a shift of the maximum of I_r , and a decrease in $T_{sr}(x)$ with increasing cerium concentration x (Figures 1–3).

For the compositions with $x = 0.93$ –0.94 (Figure 5c), the maximum of H_c progressively shifts from 25 to $\sim 10 \text{ K}$. For $x > 0.94$, the maximum shifts to 0 K and degenerates. This effect also correlates with a similar shift of the normalized K_2/K_1 ratio, shift of the maximum of I_r , and a decrease in $T_{sr}(x)$ with increasing cerium concentration x (Figures 1 and 3).

4. Conclusions

The following are our conclusions, which are inferred based on the data obtained in simulating the magnetization reversal process of the $(\text{Nd}_{1-x}\text{Ce}_x)_2\text{Fe}_{14}\text{B}$ compounds with $x = 0-1.00$ and their hysteresis loops in a wide temperature range of 300 to 0 K.

1. The model and algorithm developed for simulating the hysteresis loops of ferromagnets allow us to obtain important data on the effect of uniaxial tetragonal lattice, magnetic anisotropy parameters, and temperature dependences of the magnetic anisotropy constants on the characteristics of hysteresis loops (anisotropy field, residual magnetization, the shape of the hysteresis loop, and coercive force) in a wide temperature range.

2. Results of the simulation indicate that alloying of $\text{Nd}_2\text{Fe}_{14}\text{B}$ with cerium to its contents $x = 0.94$ (1) does not lead to the complete elimination of the negative effect of spin-reorientation phase transition on the residual magnetization of the $(\text{Nd}_{1-x}\text{Ce}_x)_2\text{Fe}_{14}\text{B}$ compounds and (2) slightly decreases the slope of the magnetization curve and almost does not lead to the improvement of the squareness of the back of hysteresis loop.

3. The alloying of $(\text{Nd}_{1-x}\text{Ce}_x)_2\text{Fe}_{14}\text{B}$ with cerium to its contents $x = 0.94$ does not allow the temperature stability of hysteretic characteristics of $(\text{Nd}_{1-x}\text{Ce}_x)_2\text{Fe}_{14}\text{B}$ -based permanent magnets to be increased in order to ensure their operation at low temperatures without losing magnetic properties.

Author Contributions: Conceptualization, N.B.K. and A.G.S.; methodology and calculations M.V.Z.; formal analysis, Y.S.K. and J.Ć.; data curation, V.P.M.; visualization, N.A.D.; writing—original draft preparation, N.B.K. and M.V.Z.; writing—review and editing, N.B.K.; writing, K.S., M.K., and P.A.P.; project administration, G.S.B. All authors have read and agreed to the published version of the manuscript.

Funding: This study was supported by the Ministry of Science and Higher Education of the Russian Federation, agreement no. 05.604.21.0244, unique identification no RFMEFI60419X0244.

Acknowledgments: The authors thank Associate V.L. Stolyarov (National University of Science and Technology MISiS) for his assistance in the program Hysteresis.

Conflicts of Interest: The authors declare no conflict of interest.

References

- Li, Z.; Liu, W.; Zha, S.; Li, Y.; Wang, Y.; Zhang, D.; Yue, M.; Zhang, J.; Huang, X. Effects of Ce substitution on the microstructures and intrinsic magnetic properties of Nd–Fe–B alloy. *J. Mag. Mag. Mater.* **2015**, *393*, 551–554. [[CrossRef](#)]
- Zhao, L.; Li, C.; Hao, Z.; Liu, X.; Liao, X.; Zhang, J.; Su, K.; Li, L.; Yu, H.; Greneche, J.-M.; et al. Influences of element segregation on the magnetic properties in nanocrystalline Nd–Ce–Fe–B alloys. *Mater. Charact.* **2019**, *148*, 208–213. [[CrossRef](#)]
- Raghavan, V. The B–Ce–Fe (Boron–Cerium–Iron) System. In *Phase Diagrams of Ternary Iron Alloys*; Indian Institute of Metals: Kolkata, India, 1992; Volume 6A, pp. 297–300.
- Herbst, J.F. $\text{R}_2\text{Fe}_{14}\text{B}$ materials: Intrinsic properties and technological aspects. *Rev. Mod. Phys.* **1991**, *63*, 819–898. [[CrossRef](#)]
- Hirosawa, S.; Matsuura, Y.; Yamamoto, H.; Fujimura, S.; Sagawa, M.; Sagawa, M.; Yamauchi, H. Magnetization and magnetic anisotropy of $\text{R}_2\text{Fe}_{14}\text{B}$ measured on single crystals. *J. Appl. Phys.* **1986**, *59*, 873–879. [[CrossRef](#)]
- Fruchart, R.; L’Heritier, P.; Dalmas de Reotier, P.; Fruchart, D.; Wolfers, P.; Coey, J.M.D.; Ferreira, L.P.; Guillen, R.; Vulliet, P.; Yaouanc, A. Mossbauer spectroscopy of $\text{R}_2\text{Fe}_{14}\text{B}$. *J. Phys. F Met. Phys.* **1987**, *17*, 483–502. [[CrossRef](#)]
- Grössinger, R.; Sun, X.K.; Eibler, R.; Buschow, K.H.J.; Kirchmayr, H.R. Temperature dependences of anisotropy fields and initial susceptibilities in $\text{R}_2\text{Fe}_{14}\text{B}$ compounds. *J. Magn. Magn. Mater.* **1986**, *58*, 55–60. [[CrossRef](#)]
- Haskel, D.; Lang, J.C.; Islam, Z.; Cady, A.; Srajer, G.; van Veenendaal, M.; Canfield, P.C. Atomic Origin of Magnetocrystalline Anisotropy in $\text{Nd}_2\text{Fe}_{14}\text{B}$. *Phys. Rev. Lett.* **2005**, *95*, 217207. [[CrossRef](#)]
- Colin, C.V.; Ito, M.; Yano, M.; Dempsey, N.M.; Suard, E.; Givord, D. Solid-solution stability and preferential site occupancy in $(\text{R}-\text{R}')_2\text{Fe}_{14}\text{B}$ compounds. *Appl. Phys. Lett.* **2016**, *108*, 242415. [[CrossRef](#)]
- Bolzoni, F.; Gavigan, J.P.; Givord, D.; Li, H.S.; Moze, O.; Pareti, L. 3d magnetism in $\text{R}_2\text{Fe}_{14}\text{B}$ compounds. *J. Magn. Magn. Mater.* **1987**, *66*, 158. [[CrossRef](#)]

11. Alam, A.; Khan, M.; McCallum, R.W.; Johnson, D.D. Site-preference and valency for rare-earth sites in $(R-Ce)_2Fe_{14}B$ magnets. *Appl. Phys. Lett.* **2013**, *102*, 042402. [[CrossRef](#)]
12. Abache, C.; Oesterreicher, J. Magnetic anisotropies and spin reorientations of $R_2Fe_{14}B$ -type compounds. *J. Appl. Phys.* **1986**, *60*, 3671. [[CrossRef](#)]
13. Hallemans, B.; Wollants, P.; Roos, J.R. Thermodynamic assessment of the Fe-Nd-B phase diagram. *J. Phase Equilib.* **1995**, *16*, 137–149. [[CrossRef](#)]
14. Li, Z.B.; Shen, B.G.; Zhang, M.; Hu, F.X.; Sun, J.R. Substitution of Ce for Nd in preparing $R_2Fe_{14}B$ nanocrystalline magnets. *J. Alloy Compd.* **2015**, *628*, 325–328. [[CrossRef](#)]
15. Wang, J.; Liang, L.; Zhang, L.T.; Yano, M.; Terashima, K.; Kada, H.; Kato, S.; Kadono, T.; Imada, S.; Nakamura, T.; et al. Mixed-valence state of Ce and its individual atomic moments in $Ce_2Fe_{14}B$ studied by soft X-ray magnetic circular dichroism. *Intermetallics* **2016**, *69*, 42–46. [[CrossRef](#)]
16. Fan, X.; Ding, G.; Chen, K.; Guo, S.; You, C.; Chen, R.; Lee, D.; Yan, A. Whole process metallurgical behavior of the high-abundance rare-earth elements LRE (La, Ce and Y) and the magnetic performance of $Nd_{0.75}LRE_{0.25}$ -Fe-B sintered magnets. *Acta Mater.* **2018**, *154*, 343–354. [[CrossRef](#)]
17. Jiang, Q.; Zhong, Z. Research and development of Ce-containing $Nd_2Fe_{14}B$ -type alloys and permanent magnetic materials. *J. Mater. Sci. Technol.* **2017**, *33*, 1087–1096. [[CrossRef](#)]
18. Pei, K.; Zhang, X.; Lin, M.; Yan, A.R. Effects of Ce-substitution on magnetic properties and microstructure of Nd-Pr-Fe-B melt-spun powders. *J. Magn. Magn. Mater.* **2016**, *398*, 96–100. [[CrossRef](#)]
19. Yan, C.; Guo, S.; Chen, R.; Lee, D.; Yan, A. Effect of Ce on the Magnetic Properties and Microstructure of Sintered Didymium-Fe-B Magnets. *IEEE Trans. Magn.* **2014**, *50*, 2102605. [[CrossRef](#)]
20. Pathak, A.K.; Gschneidner, K.A.; Khan, M.; McCallum, R.W.; Pecharsky, V.K. High performance Nd-Fe-B permanent magnets without critical elements. *J. Alloys Compd.* **2016**, *668*, 80–86. [[CrossRef](#)]
21. Fuerst, C.D.; Herbst, J.F.; Sarrao, J.L.; Migliori, A. Resonant ultrasound measurements of elastic constants of melt-spun of $R_2Fe_{14}B$ compounds ($R=Ce, Pr, Nd, Er$). *J. Appl. Phys.* **1994**, *75*, 6625–6627. [[CrossRef](#)]
22. Susner, M.A.; Conner, B.S.; Saporov, B.I.; McGuire, M.A.; Crumlin, E.J.; Veith, G.M.; Cao, H.; Shanavas, K.V.; Parker, D.S.; Chakoumakos, B.C.; et al. Flux growth and characterization of Ce-substituted $Nd_2Fe_{14}B$ single crystals. *J. Mag. Mag. Mater.* **2017**, *434*, 1–9. [[CrossRef](#)]
23. Menushenkov, V.; Savchenko, A.; Stoliarov, V.; Zheleznyi, M.; Kolchugina, N.; Dormidontov, N.; Skotnicova, K.; Koshkidko, Y. Simulation of demagnetization reversal and hysteretic loops of $(Nd, Pr)_2Fe_{14}B$ magnets at low temperatures. In *Proceedings of 28-th International Conference on Metallurgy and Materials, Metal 2019, Brno, Czech Republic, 22–24 May 2019*; Tanger Ltd.: Ostrava, Czech Republic, 2019; pp. 1621–1627.
24. Jiang, S.; Li, H.; Xu, J.; Gao, R. Research on the origin of magneto-crystalline anisotropy in $R_2Fe_{14}B$ compounds. *J. Mag. Mag. Mater.* **1994**, *136*, 294–300.
25. Xu, W.G.; Liu, Y.L.; Ji, S.Q.; Chu, D.P.; Xu, Y.; Yang, G.L. Temperature dependence of the anisotropy constants K_1 and K_2 of $R_2Fe_{14}B$ ($R = Ce, Pr, Gd$). *Acta Sin.* **1986**, *35*, 1592–1597.

